Journal of Ceramic Processing Research. Vol. 13, No. 6, pp. 810~815 (2012)

J O U R N A L O F
Ceramic Processing Research

Microstructural analysis of the functionally graded electrodes in solid oxide fuel cells

Seoung-Ju Lee[a], Chi-Young Jung[b] , Kwang-Bo Shim[c] and Sung-Chul Yi[a,b]*

[a]*Department of Hydrogen and Fuel Cell Technology, Hanyang University, Haengdang-dong, Seongdong-gu, Seoul 133-791, Korea*
[b]*Department of Chemical Engineering, Hanyang University, Haengdang-dong, Seongdong-gu, Seoul 133-791, Korea*
[c]*Department of Materials Science and Engineering, Hanyang University, Haengdang-dong, Seongdong-gu, Seoul 133-791, Korea*

The active surface area is an important factor in improving the cell performance of a solid oxide fuel cell (SOFC). An electrochemical analysis incorporating an active surface area was performed to account for the effect of grading, which affects both the active surface area and the effective diffusivity within the electrodes. The analysis showed the good agreement with experimental data from the literature and used to predict the cell polarizations in porosity-graded and particle-size graded electrodes. The particle-size graded electrode demonstrated better cell performance than the porosity-graded electrode, due to a larger active surface area. Detailed studies were performed to investigate the effect of particle-size variation. As a result, the graded functional layers demonstrated improved performance than the base case with a fixed average porosity. Consequently, it can be concluded that the overall cell polarization was mainly affected by lowered activation overpotentials when the particle-size grading was conducted.

Key words: SOFC, Functionally graded electrode, Model, Functional layer.

Introduction

Solid oxide fuel cells (SOFCs) are very attractive as an alternative power source for stationary applications, due to low emissions and high efficiency. It can also be fueled with hydrocarbon fuels, such as methane (CH_4) or ethane, instead of hydrogen (H_2). During the last decade, the number of literatures on SOFC has grown because of the increased public interest in their commercialization [1-2].

In the field of SOFC engineering, the properties involving microstructures of the electrodes have been regarded as the important factors to enhance reaction kinetics and overall cell polarizations [3]. A number of scientific papers on the microstructure engineering of the SOFCs have been published [4-17]. When electrochemical reactions are involved, the amount of charge generation or depletion is dependent on the active surface area in the electrodes [4]. To properly incorporate the influences of electrode-microstructural changes, microscopic configurations in the electrodes should be coupled with a conventional macroscopic modeling. Costamagna et al. [5] developed an analytical model that describes the response of an electrode characterized by two continuous solid interlaced structures. Their model evaluated the electrode performance as a function of the electrode morphology and composition. After that, Virkar et al. [6] discussed the effects of electrode microstructure on the activation and concentration potential losses in the SOFC and introduced the concept of effective charge transfer resistance. Chan et al. [7] presented a complete polarization model of SOFC that could work under multiple design and operating conditions. Sorrentino et al. [8] built a one-dimensional (1-D) model for a planar SOFC and validated it with the experimental data from the Pacific Northwest National Laboratory. Furthermore, Hussain et al. [9] and Ni et al. [10] have reported on 1-D planar SOFC models by coupling microscopic electrode models.

Besides, there is a rising scientific interests on functionally graded electrodes in a SOFC. As illustrated in Fig. 1, the functionally graded electrode is microstructurally-engineered electrode, which includes high active surface area at electrode-electrolyte interface. Ni et al. [11] has explored linearly graded electrodes with particle sizes and porosities. Holtappels et al. [12] presented linearly graded SOFC anode with porosities to improve fuel mass transport limitation through the electrode. After that, the linearly gradings of porosity [13-14] and compositions [15-16] were conducted to optimize electrode microstructures. Recently, McCoppin et al. [17] introduced a novel spraying technique to fabricate continuously graded anode functional layer. However, none of them attempted to explore electrode properties with second-order profiles.

In this paper, an isothermal and one-dimensional (1-D) model was developed and implemented using a microstructure-involved relationship proposed by Costamagna et al. [5]. To evaluate the grading effects in electrode by means of mathematical modeling, a coupling of microscopic and macroscopic models

*Corresponding author:
Tel : +82-2-2220-0481
Fax: +82-2-2298-5147
E-mail: scyi@hanyang.ac.kr

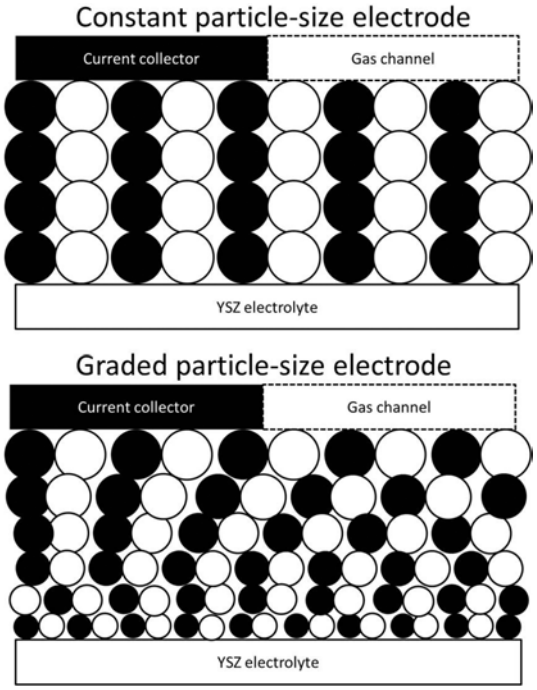

Fig. 1. Schematic of the graded particle-size electrode.

should is crucial. The main purpose of this paper was to investigate the particle-size grading effects. Simulated polarization data of the base design were validated using experimental data from the literature. In addition, the influences of the linear and second-order graded functional layers on cell polarization were investigated with fixed averaged porosity.

Model Formulation

Description of the SOFC model

A cross-sectional 1-D positive-electrolyte-negative (PEN) assembly model was used for computational analysis. A five-layered PEN assembly including an anode backing layer (ABL), an anode functional layer (AFL), a yttria-stabilised zirconia (YSZ) electrolyte, a cathode functional layer (CFL) and a cathode backing layer (CBL) is illustrated in Fig. 2.

The major assumptions made to formulate the model are listed below:

i) Steady-state operation
ii) Isothermal conditions
iii) Ideal gas mixture
iv) Negligible convective flux
v) Solid- and electrolyte-phase potentials that were used to describe electron and proton transport, respectively

Transport in the microstructured electrodes

The transport of multi species, including H_2, O_2 and H_2O, occurs within the porous electrodes, as they are generated or depleted by the electrochemical reactions at the FLs.

The governing equation for species transfer can be

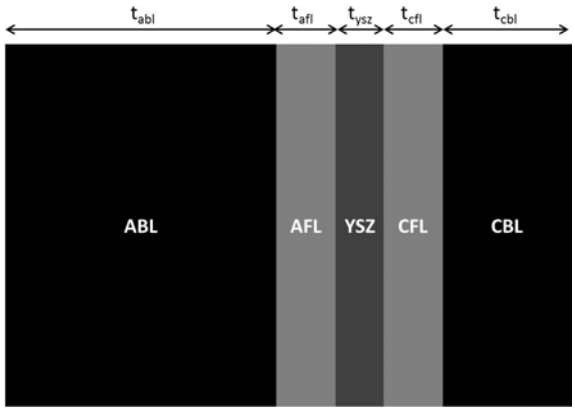

Fig. 2. A shematic of the cross-section region of the PEN assembly in an anode-supported SOFC.

written as [18]:

$$0 = \nabla \cdot \left(\frac{\varepsilon}{\tau} D_i^{eff} \nabla C_i \right) + S_i \tag{1}$$

where ε, τ, C_i and S_i are the porosity, tortuosity, molar concentration of species i and the generation or depletion rate by electrochemical reaction, respectively.

In porous electrodes, the diffusion can be proceed by molecular or Knudsen diffusion, depending on the mean free path of the gas molecule. Generally, both molecular and Knudsen diffusion are comparable under the operating conditions used in SOFC. The effective diffusion coefficient, considering pore structure and the two diffusion mechanisms, can be defined as [18]:

$$D_i^{eff} = \frac{D_i D_{K,i}}{D_i + D_{K,i}} \tag{2}$$

where D_i and $D_{K,i}$ are the bulk and the Knudsen diffusion coefficient of species i, respectively. The Knudsen diffusion coefficient of species i, $D_{K,i}$, can be calculated as follows:

$$D_{K,i} = \frac{1}{3} d_p \sqrt{\frac{8RT}{\pi M_i}} \tag{3}$$

where d_p, M_i, R and T are the pore diameter, molecular weight of species i, universal gas constant and operating temperature, respectively.

The source/sink term arising from the electrochemical reactions, e.g., the HOR or ORR, S_i, can be calculated by Eq. 4.

$$S_i = \frac{\xi_i \nabla \cdot I}{n_i F} \tag{4}$$

where ξ_i, $\nabla \cdot I$ and F are the stoichiometric coefficient, rate of charge generation/depletion and the Faraday constant, respectively.

Electrochemical reactions in the microstructured electrodes

The rates of the HOR and ORR are dominated by Butler-Volmer kinetics in the AFL and CFL, respectively.

The amount of charge generation can be calculated as below [19]:

$$\nabla \cdot I_a = A_V i_{0,H_2} \left(\frac{C_{H_2}}{C_{H_2,ref}} \right)^{0.5} \times \left\{ \exp\left(\frac{F\eta_a}{RT} \right) - \exp\left(\frac{F\eta_a}{RT} \right) \right\} \quad (5)$$

$$\nabla \cdot I_c = A_V i_{0,O_2} \left(\frac{C_{O_2}}{C_{O_2,ref}} \right)^{0.5} \times \left\{ \exp\left(\frac{F\eta_c}{RT} \right) - \exp\left(\frac{F\eta_c}{RT} \right) \right\} \quad (6)$$

where i_{0,H_2}, i_{0,O_2}, $C_{H_2,ref}$ and $C_{O_2,ref}$ represent the HOR exchange current density, ORR exchange current density, reference H_2 concentration and reference O_2 concentration, respectively. The anode and cathode overpotential, η, is defined as follows:

$$\eta = \Phi_s - \Phi_e \quad (7)$$

The active surface area per unit volume A_v, depends on the microstructure of the components the reaction zone. In this study, A_v is calculated using the following expression [14]:

$$A_v = \pi \sin^2\theta r_{el}^2 n_t n_{el} n_{io} \frac{Z_{el} Z_{io}}{Z} P_{el} P_{io} \quad (8)$$

where θ, r_{el}, n_t, n_{el} and n_{io} are the contact angle between electron and ion-conducting particles, the radius of the electron-conducting particles, the number of particles per volume, and the number fraction of the electron- and ion-conducting particles, respectively. Z, Z_{el} and Z_{io} are the average coordination number and the coordination number of electron- and ion-conducting particles, respectively. In addition, P_{el} and P_{io} are the probabilities of the electron- and ion-conducting particles, respectively. The parameters in Eq. 8 can be calculated using the Eqs. 9-16.

$$n_t = \frac{1-\varepsilon}{\frac{4}{3}\pi r_{el}^3 \left[n_{el} + (1-n_{el}) \left(\frac{r_{io}}{r_{el}} \right)^3 \right]} \quad (9)$$

$$n_{el} = \frac{\varphi}{\left[\varphi + (1-\varphi) \left(\frac{r_{io}}{r_{el}} \right)^3 \right]} \quad (10)$$

$$Z_{el} = 3 + \frac{Z-3}{\left[n_{el} + (1-n_{el}) \left(\frac{r_{io}}{r_{el}} \right)^2 \right]} \quad (11)$$

$$Z_{io} = 3 + \frac{(Z-3)\left(\frac{r_{io}}{r_{el}} \right)^2}{\left[n_{el} + (1-n_{el}) \left(\frac{r_{io}}{r_{el}} \right)^2 \right]} \quad (12)$$

$$P_{el} = \left[1 - \left(\frac{4.236 - Z_{el-el}}{2.472} \right)^{2.5} \right]^{0.4} \quad (13)$$

$$P_{io} = \left[1 - \left(\frac{4.236 - Z_{io-io}}{2.472} \right)^{2.5} \right]^{0.4} \quad (14)$$

$$Z_{el-el} = \frac{n_{el} Z}{n_{el} + (1-n_{el}) \left(\frac{r_{io}}{r_{el}} \right)^2} \quad (15)$$

$$Z_{io-io} = \frac{n_{io} Z_{io}^2}{Z} \quad (16)$$

Computational method

All governing equations and boundary conditions for each variable were used to numerically simulate the presented model using FLUENT, a CFD software package based on the finite volume method [20]. Because FLUENT does not contain an electrochemical modeling module and the source terms in the model are highly nonlinear, all governing equations were modeled using user defined functions (UDFs) [21]. To mitigate the nonlinearity due to the severe coupling and to increase the rate of convergence, all simulations were performed from high to low cell potential, in sequence, using the computational data from the previous case as the initial data [22-23].

Results and Discussions

Model validation

To confirm the validity of the developed model, the simulation results were compared with experimental data available in the literature. The predicted cell performance showed good agreement with measured data from Rogers et al. [24], as shown in Fig. 3. The parameters and operating conditions used in this study were mostly derived from Rogers et al., except for a few parameters, such as particle size, volumetric fraction of the particle and exchange current density. The unavailable parameters were taken from Hussain et al. [19], and these parameters are listed in Table 1. To find a best fit curve, the electrode tortuosity was adjusted to a value in the typical range of 2-6 [25]. A final tortuosity value of 2.0 was chosen and fixed.

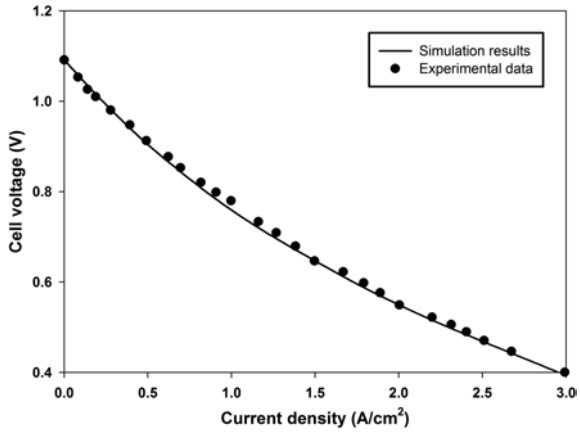

Fig. 3. Comparison between the simulation and the experimental data [24].

Table 1. Parameters used in the model validation [19, 24]

Parameter	Value
Operating temperature (K), T	1073
Operating Pressure (atm), P	1
Anode-inlet mole fraction, X_{H_2}, X_{H_2O}	0.95, 0.05
Cathode-inlet mole fraction, X_{O_2}, X_{N_2}	0.79, 0.21
Anode conductivity (S m^{-1}), σ_a	71428.57
Cathode conductivity (S m^{-1}), σ_c	5376.34
Electrolyte conductivity (S m^{-1}), σ_{ysz}	0.64
Anode backing layer thickness (m), t_{abl}	1.0×10^{-3}
Anode functional layer thickness (m), t_{afl}	2.0×10^{-5}
YSZ electrolyte thickness (m), t_{ysz}	1.0×10^{-5}
Cathode functional layer thickness (m), t_{cfl}	2.0×10^{-5}
Cathode backing layer thickness (m), t_{cb}	5.0×10^{-5}
Porosity of anode and cathode, ε	0.375
Tortuosity of anode and cathode, τ	2.0
Pore diameter of anode and cathode (m), d_p	1.5×10^{-6}
Contact angle between electron- and ion-conducting particles (^{o}), θ	15
Radius of electron-conducting particle (m), r_{el}	1×10^{-7}
Radius of ion-conducting particle (m), r_{io}	1×10^{-7}
Volume fraction of electron-conducting particle, φ	0.5
Reference H_2 concentration (mol m^{-3}), $C_{H_2,ref}$	10.78
Reference O_2 concentration (mol m^{-3}), $C_{O_2,ref}$	2.38
Reference exchange current density for H_2 oxidation (A m^{-2}), i_{0,H_2}	1320
Reference exchange current density for O_2 reduction (A m^{-2}), i_{0,O_2}	400

Functionally graded electrodes

Fig. 4 shows the cell polarizations with different electrode microstructures. The design parameters of the base case are given in Table 1. The electrode of the base case has both homogeneous porosity and particle-size. The porosity, ranging from 0.3-0.7, and the particle-size, ranging from 0.01-5.0 μm, were used for a linearly graded electrode. As shown in Fig. 4, the linearly graded electrodes had better performances than the base case, especially in the case of a particle-size graded electrode. With porosity-graded and particle-size graded electrodes, the current density at 0.6 V increased by 6% and 45%, respectively, when compared with the base case.

Fig. 5 shows the variations of active surface area per unit volume within the AFL, demonstrating the significant differences between the porosity-graded and the particle-size graded electrodes. These differences are most likely due to the variations of the active surface area in a linear and an exponential manner for the porosity-graded and the particle-size graded cases,

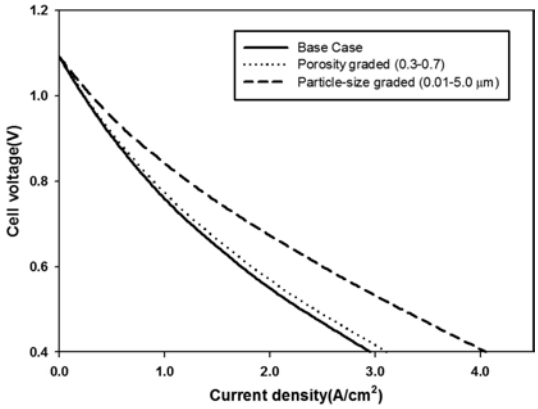

Fig. 4. The comarison among the base case and linearly graded electrodes.

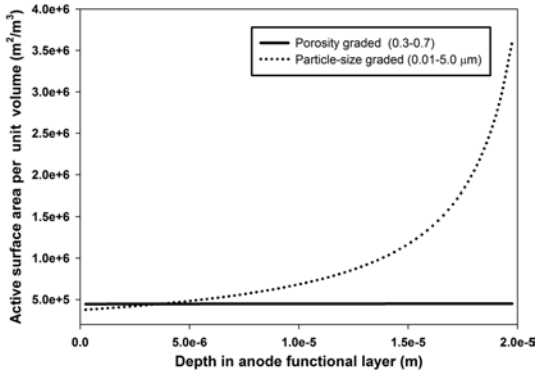

Fig. 5. Active surface area per unit volume within AFL.

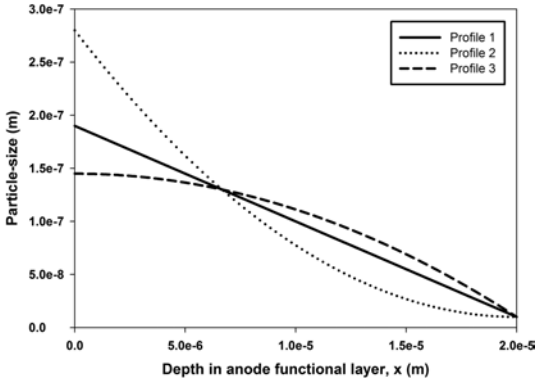

Fig. 6. Three modes of grading profiles when $\varepsilon_{ave} = 0.4$

respectively. The particle-size graded electrode had a larger active surface area than the porosity-graded electrode in the given grading ranges. Consequently, the particle-size graded electrode was more effective at improving cell performance, as shown in Fig. 4.

Linearly graded and second-order graded electrodes

Electrochemical reactions in the SOFCs mostly occur near the electrode-YSZ interface [1], making the microstructure of the FL a major factor in cell polarisation. To study the effects of particle-size grading in the FL, several cases were investigated. For the three grading profiles, given in Fig. 6, the average

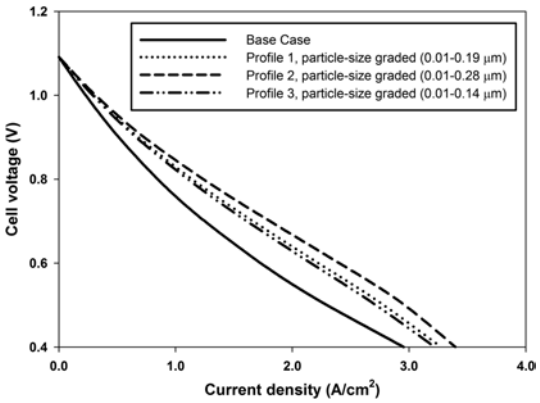

Fig. 7. Cell polarizations with different grading profiles.

porosity ε_{ave}, in the AFL was fixed for each case to focus on the grading effect without the influence of quantitative change on the AFL porosity. Profile 1 is a linearly graded case, which was used in Fig. 4. Profile 2 and 3 are 2nd-order graded cases. The profiles could be expressed as:

Profile 1: $-ax + b$
Profile 2: $a(x - c)^2 + b$
Profile 3: $-ax^2 + b$

where a and b are constants determined by the grading range and targeted average porosity; c is the distance between the start and the end point of the x axis. The ABL-AFL interface is at $x = 0$, and the AFL-YSZ interface is the end of the x axis.

The polarization variation with an average AFL porosity of 0.4 is presented in Fig. 7; the linearly graded and 2nd-order graded cases are compared with the base case. As seen in the figure, the cell polarizations of all profiles suggested for grading particle sizes in the FL were improved compare to the base case. Among the suggested profiles, the profile 2 presented the most enhanced performance, resulting in approximately 30% more current density than the base case at 0.6 V. Especially, cell polarizations in low-current region, ranging from 0 to 0.5 A cm^{-2} showed remarkable difference among particle-size graded and nongraded cases, while the ohmic slopes at intermediate-current region was quite similar. According to the Fig. 5, this is mainly because of differences in the active surface area.

Conclusions

An electrochemical model accounting for an active surface area was developed to characterize the cell performance of a graded electrode in a SOFC. We evaluated the validity of the model with experimental data from the literature and investigated the effects on both a porosity-graded and a particle-size graded electrode. Both cases were improved by cell polarization. However, the large active surface area in the particle-size graded electrode case resulted in better cell performance than the porosity-graded electrode case.

Because particle-size grading has significant impact on cell polarization due to increase of the active surface area, detailed studies were performed to explore the effects of particle-size variation. The cell performance was increased when a graded FL was employed. From the results, particle-size grading can be regarded as effective method for preparation of the FLs. However, it should be noted that the cell performance can be varied with different grading profiles. Our work suggests that even a small amount of paricle-size variation, ranging from 0.01 to 0.28 μm, can be a major factor when preparing the FLs of the SOFCs.

Acknowledgements

This work was supported by the Manpower Development Program for Energy & Resources funded by the Ministry of Knowledge and Economy, Republic of Korea. It was also partially supported by Solid oxide fuel cell of New & Renewable Energy R & D program (20093021030010) under the Korea Ministry of Knowledge Economy (MKE).

Nomenclature

a	Constant for grading profile
A_v	Active surface area per unit volume (m^2 m^{-3})
b	Constant for grading profile
c	Constant for grading profile
C	Molar concentration (mol m^{-3})
d_p	Pore diameter (m)
D	Diffusion coefficient (m^2 s^{-1})
F	Faraday constant (96485 C mol^{-1})
i_0	Exchange current density (A m^{-2})
I	Current density (A m^{-2})
M	Molecular weight (kg mol^{-1})
n_{el}	Number fraction of electron-conduction particles
n_i	Number of electrons transferred per reaction
n_{io}	Number fraction of ion-conduction particles
n_t	Total number of particles in unit volume (m^{-3})
r	Radius of particles (m)
R	Universal gas constant (8.314 J mol^{-1} K^{-1})
S	Source term (mol m^{-3} s^{-1})
p	Probability of percolation
P	Pressure (atm)
t	Thickness (m)
T	Temperature (K)
x	Coordinate
X	Mole fraction
Z	Average coordination number
Z_{el}	Coordination number of electron-conducting particles
Z_{io}	Coordination number of ion-conducting particles

Greek letters

ε	Porosity

η	Over potential (V)
θ	Contact angle between electron and ion-conducting particles (^{o})
ξ	Stoichiometric coefficient
σ	Charge conductivity (S m^{-1})
τ	Tortuosity
φ	Volume fraction of electron-conducting particles
Φ	Charge potential (V)

Subscripts & superscripts

a	Anode
abl	Anode backing layer
afl	Anode functional layer
ave	Average
c	Cathode
cbl	Cathode backing layer
cfl	Cathode functional layer
e	Electrolyte phase
el	Electron-conducting particles
eff	Effective
i	Species
io	Ion-conducting particles
K	Knudsen diffusion
ref	Reference
s	Solid phase
ysz	YSZ-electrolyte

Abbreviation

ABL	Anode backing layer
AFL	Anode functional layer
CBL	Cathode backing layer
CFD	Computational fluid dynamic
CFL	Cathode functional layer
FL	Functional layer
HOR	Hydrogen oxidation reaction
ORR	Oxygen reduction reaction
PEN	Positive electrode-electrolyte-negative electrode
SOFC	Solid oxide fuel cell
YSZ	Yttria stabilised zirconia

References

1. S.C. Singhal, K. Kendall, in "High temperature solid oxide fuel cells: fundamentals design and applications" Elsevier Ltd. (2004) Chap. 1.
2. J. Larminie, A. Dicks, in "Fuel cell systems explained" (John Wiley and Sons Ltd., 2003) Chap. 1-2.
3. J.-H. Cha, Y.-C. Chung, H.-R. Kim, J.-W. Son, J. Kim, J.-H. Lee, H.-W. Lee, J. Ceram. Process. Res. 8 (2007) 224-228.
4. J.C. Ordonez, S. Chen, J.V.C. Vargas, F.G. Dias, J.E.F.C. Gardolinski and D. Vlassov, Int. J. Energ. Res. 31 (2007) 1337-1357.
5. P. Costamagna, P. Costa and V. Antonucci, Electrochim. Acta 43 (1998) 375-394.
6. A.V. Virkar, J. Chen, C.W. Tanner and J.W. Kim, Solid State Ionics 131 (2000) 189-198.
7. S.H. Chan, K.A. Khor, Z.T. Xia, J. Power Sources 93 (2001) 130-140.
8. M. Sorrentino, A. Mandourah, T.F. Petersen, Y.G. Guezennec, M.J. Moran and G. Rizzoni, in Proceedings of the 2004 ASME International Mechanical Engineering Congress and Exposition, November 2004.
9. M.M. Hussain, X. Li, I. Dincer, J. Power Sources 161 (2006) 1012-1022.
10. M. Ni, M.K.H. Leung and DYC Leung, Fuel Cells 7 (2007) 269-278.
11. M. Ni, M.K.H. Leung and DYC Leung, J. Power Sources 168 (2007) 369-378.
12. P. Hotappels, C. Sorof, M.C. Verbraeken, S. Rambert, U. Vogt, Fuel Cells 6 (2006) 113-116.
13. E.S. Greene, W.K.S. Chiu, M.G. Medeiros, J. Power Sources 161 (2006) 225-231.
14. A. Bertei, C. Nicolella, J. Power Sources 196 (2011) 9429-9436.
15. J. Deseure, L. Dessemond, Y. Bultel, E. Siebert, J. Eur. Ceram. Soc. 25 (2005) 2673-2676.
16. L.C.R. Schneider, C.L. Martin, Y. Bultel, L. Dessemond, D. Bouvard, Electrochim. Acta 52 (2007) 3190-3198.
17. J. McCoppin, I. Barney, S. Mukhopadhyay, R. Miller, T. Reitz, D. Young, J. Power Sources 215 (2012) 160-163.
18. R.B. Bird, W. Stewart and E.N. Lightfoot, in "Transport phenomena" (Wiley, 1973) Chap. 17-19.
19. M.M. Hussain, in "Multi-component and multi-dimensional mathematical modeling of solid oxide fuel cells" (Ph.D. dissertation, Waterloo Univ., 2008) Chap. 2-3.
20. S.V. Patankar, in "Numerical heat transfer and fluid flow" (Hemisphere Publishing Corp. 1980) 13-52.
21. Fluent, in "Fluent 6.3 UDF Guide", (Fluent Inc.) Chap. 1-3.
22. C.-Y. Jung, H.-S. Shim, S.-M. Koo, S.-H. Lee and S.-C. Yi, Appl. Energ. 93 (2012) 733-741.
23. C.-Y. Jung, W.-J. Kim and S.-C. Yi, Int. J. Hydrogen Energ. 37 (2012) 7654-7668.
24. W.A. Rogers, R.S. Gemmen, C. Johnson, M. Prinkey and M. Shahnam, Fuel Cell Sci. Eng. Technol. ASME (2003) 517-520.
25. R.E. Williford, L.A. Chick, Surface Science 547 (2003) 421-437.